

Nanoscale Advances

Accepted Manuscript

This article can be cited before page numbers have been issued, to do this please use: J. Jose, A. J. Mathew, E. Gabriel, A. James and T. P. Vinod, *Nanoscale Adv.*, 2026, DOI: 10.1039/D5NA01139F.



This is an Accepted Manuscript, which has been through the Royal Society of Chemistry peer review process and has been accepted for publication.

Accepted Manuscripts are published online shortly after acceptance, before technical editing, formatting and proof reading. Using this free service, authors can make their results available to the community, in citable form, before we publish the edited article. We will replace this Accepted Manuscript with the edited and formatted Advance Article as soon as it is available.

You can find more information about Accepted Manuscripts in the [Information for Authors](#).

Please note that technical editing may introduce minor changes to the text and/or graphics, which may alter content. The journal's standard [Terms & Conditions](#) and the [Ethical guidelines](#) still apply. In no event shall the Royal Society of Chemistry be held responsible for any errors or omissions in this Accepted Manuscript or any consequences arising from the use of any information it contains.

ARTICLE

Fluorescent Nanocellulose Derived from *Plectranthus barbatus* for the Selective Detection of Pb (II) Ions in Aqueous SolutionsJoshua Jose,^{*a} Aishwarya Joji Mathew,^a Elizabeth Gabriel,^a Ancilin James,^a and Vinod T. P. ^{*a, b}Received 00th January 20xx,
Accepted 00th January 20xx

DOI: 10.1039/x0xx00000x

This study reports the synthesis of fluorescent nanocellulose from the *Plectranthus barbatus* and its effective use as a fluoroprobe for the detection of Pb (II) ions in aqueous solutions. Nanocellulose, a nanoscale derivative of cellulose, are used in a variety of applications, such as sensing, food packaging, and biomedical applications, owing to its characteristic properties. In sensing applications, they are mostly used as a support or substrate for the sensing probe. Nanocellulose shows intrinsic fluorescence, which can be harnessed for sensing applications. This underexplored research domain holds significant potential for developing sustainable and cost-effective sensing materials. We synthesized nanocellulose from *Plectranthus barbatus* (PBNC) and employed it as a fluorescent probe for the detection of Pb (II). To the best of our knowledge, this is the first report demonstrating the potential of fluorescent nanocellulose for metal ion detection. The properties of fluorescent nanocellulose, PBNC, were studied using Fourier Transformation Infrared (FTIR) spectroscopy, X-ray Diffraction (XRD), Transmission Electron (TEM) Microscopy, and Photoluminescence (PL) spectroscopy. The fluorescent intensity of the nanocellulose was remarkably quenched in the presence of Pb (II) ions selectively. The detection limit (LOD) of Pb (II) using PBNC was found to be 2.7 nM. PBNC is a novel autofluorescent material that functions as an efficient nanosensor for the detection of Pb (II) ions, and its applications can be extended to bio-imaging and sensing in biological, chemical, and environmental samples.

1. Introduction

Cellulose, a plant-based polysaccharide, is composed of polymerized β -D-glucopyranose units that form a distinctive structural framework.¹ Miniaturization of cellulose results in the formation of nanocellulose or cellulose nanomaterials, which exhibit enhanced structural, mechanical, and optical properties, thereby broadening their spectrum of applications.² Nanocellulose is widely used in biosensors and chemical sensors owing to the abundance of functional groups, high surface area, and flexibility.³ In most of their applications in sensors, nanocellulose is used as a substrate to host the probe material.⁴ Nanocellulose is not considered an active sensor component, as it generally lacks the optical and electrochemical properties required to generate and acquire analytical responses.⁵ Contrary to the common perception of nanocellulose as an inert material with respect to signal generation, recent findings reveal that it exhibits intrinsic autofluorescence, thereby unlocking new potential for sensor applications. Autofluorescence in nanocellulose is an inherent property, without any fluorescent labels or impurities added to it.⁶ The cause of autofluorescence in nanocellulose is still obscure, as

there are no aromatic groups or π -conjugation in its structure, which is considered to be a prerequisite for photoluminescence in organic compounds.⁷ The most prominent theory regarding autofluorescence in nanocellulose is clustering-triggered emission (CTE).⁸ According to this theory, the electron-rich functional groups (carbonyls, hydroxyls, etc.) in the nanocellulose interact through space, thereby reducing the band gap of nanocellulose, resulting in emissions.⁹ In nanocellulose, the abundant oxygen-rich groups, along with the presence of hydrogen bonds, are considered to be manifesting the fluorescence.¹⁰ Autofluorescence of nanocellulose remains an underexplored phenomenon, which offers significant and untapped potential for sensing applications. They have the potential to be used efficiently and effectively in heavy metal ion detection, environmental monitoring, biomedical engineering and in food safety analysis.¹¹

Plectranthus barbatus was selected as the precursor for the synthesis of nanocellulose owing to its high content of polyphenols and flavonoids, which can function as intrinsic fluorophores or fluorescence-enhancing agents upon conversion to nanocellulose.¹² This inherent phytochemical richness supports the development of environmentally benign, green fluorescent sensing platforms. Furthermore, the abundance of oxygen-containing functional groups provides effective coordination sites for Pb(II) ions, contributing to enhanced selectivity toward Pb(II).¹³ In addition, *Plectranthus barbatus* is inexpensive, renewable, and widely available,

^a Department of Chemistry, Christ University, Hosur Road, Bengaluru 560029, India.^b Centre for Renewable Energy and Environmental Sustainability, Christ University, Bengaluru 560029, India

* E-mail: vinod.tp@christuniversity.in

Supplementary Information available: [details of any supplementary information available should be included here]. See DOI: 10.1039/x0xx00000x



rendering it a sustainable lignocellulosic feedstock for scalable nanocellulose production.¹⁴

In the present study, we synthesized a novel autofluorescent nanocellulose from the *Plectranthus barbatus* plant through optimised pretreatment and acid hydrolysis procedures. The autofluorescent *Plectranthus barbatus* nanocellulose (PBNC) was used as a fluoroprobe for the detection of Pb (II) ions in aqueous solutions. The nanocellulose showed good selectivity towards Pb (II) ions with a detection limit of 2.7 nM. To the best of our knowledge, this work represents the first report on the application of autofluorescent nanocellulose for the detection of Pb (II) ions. The sensitivity, selectivity, and simplicity of this sensor system are comparable to other nanocellulose-based systems, offering a novel and effective strategy for the fluorescent detection of a highly toxic heavy metal.

2. Materials and Methods

2.1 Chemicals

Plectranthus barbatus plant was collected from Begur village, Bengaluru, India. Sodium hydroxide (NaOH), Hydrogen peroxide (H₂O₂), Sulphuric acid (H₂SO₄), Quinine sulphate (QS), MnSO₄, BaCl₂, NiSO₄, HgCl₂, AlCl₃, FeCl₂, NaCl, PbCl₂, Na₂HPO₄·12H₂O, and NaH₂PO₄, were purchased from Sigma Aldrich. Syringe filters (Nylon, pore size 0.22 μm) and Dialysis membrane-70 (Flat width -28.46 mm, Diameter -17.5 mm, molecular weight cut-off of 1200 Da to 1400 Da) were procured from HiMedia Laboratories, India.

2.2 Synthesis of *Plectranthus barbatus* Nanocellulose (PBNC)

2.2.1 Pretreatment of *Plectranthus barbatus* Plant

The *Plectranthus barbatus* plant was subjected to alkali treatment and bleaching in order to remove the lignin and hemicellulose content, using previously reported procedures.^{15,16} The *Plectranthus barbatus* plant was first cleaned and thoroughly washed with water and then dried in sunlight for two days. Then it was grounded into powder form and dried. 5 g of the powder was weighed and added to 100 ml of 5% (w/v) NaOH solution. The mixture was then stirred for one hour at 75°C. The resultant reaction mixture was washed with water until a neutral pH was reached and then dried. This step is crucial in the delignification process of the fiber, as it determines the quality and color of the resulting cellulose. The delignified sample was added to 100 ml of a solution containing 4% NaOH (w/w) and 24% hydrogen peroxide (v/v) in a 1:1 ratio, and the mixture was stirred vigorously for two hours. The resulting residue was then washed with water and sun dried to obtain the *Plectranthus barbatus* cellulose.

2.2.2 Preparation of *Plectranthus barbatus* Nanocellulose (PBNC)

PBNC was prepared by the acid hydrolysis of *Plectranthus barbatus* cellulose, using previously reported procedures.^{15,17} 5 g of *Plectranthus barbatus* cellulose was added to 100 ml of 35 % (w/w) sulfuric acid. The mixture was then subjected to magnetic stirring for three hours at room temperature. Distilled

water was added to the solution to stop the reaction. Following this, it was centrifuged for three cycles at 8500 rpm, with each cycle lasting 20 minutes. Following centrifugation, the acidic supernatant was removed and replaced with distilled water. The nanocellulose suspension was syringe filtered to remove residual matter. The resultant solution was then subjected to dialysis for 24 hours to remove acid residues. The nanocellulose collected from the membrane was vigorously stirred for 10 minutes to break down the particles. The resultant PBNC was then collected, refrigerated and used for characterization.

2.3 Characterizations

Fourier transform infrared (FTIR) spectra with a frequency range of 4000 to 500 cm⁻¹, and a spectral resolution of 4 cm⁻¹ were obtained from the samples using a Perkin Elmer Spectrum 100 spectrometer. A Bruker D Advance X-ray diffractometer (XRD) was used to perform the X-ray diffraction investigation using Cu-Kα radiation with a wavelength of 1.5406 Å. The operating conditions of the diffractometer were set at 40 kV and 20 mA, and data were collected with a range of 10 to 90 degrees. Scanning electron microscopy (SEM) images were obtained utilizing the Thermo Fisher Scientific, Apreo 2S, with a maximum accelerating voltage of 30 kV. High-resolution transmission electron microscopy (HRTEM) images were acquired using the JEOL JEM-2100, LaB6, operating at 200 kV. The suspension's zeta potential was measured by dynamic light scattering (DLS) with a Zetasizer (ZS90) instrument. The optical properties of the nanocellulose were recorded using a UV-vis spectrophotometer (Shimadzu UV-1500) and fluorophotometer (Shimadzu RF-6000). PL lifetime measurements were recorded using a JOBIN-VYON M/S Fluorocube system.

2.4 Quantum Yield (ϕ) Calculation

The quantum yield of PBNC was calculated by the reference method using quinine sulphate (ϕ = 54%) in 0.1 M H₂SO₄ as the reference.¹⁸ The absorbance of aqueous solutions of the PBNC and the quinine sulphate was measured by keeping the optical density below 0.1 at a wavelength of 220 nm. Afterwards, the fluorescence intensities of reference and PBNC were determined. The quantum yield for PBNC was calculated using the following equation.

$$\phi_S = \phi_R \left(\frac{I_S}{I_R} \right) \cdot \left(\frac{A_R}{A_S} \right) \cdot \left(\frac{\eta_S^2}{\eta_R^2} \right)$$

where,

ϕ_S	Quantum yield of the sample
ϕ_R	Quantum yield of the reference
I_S	Fluorescence intensity of the sample
I_R	Fluorescence intensity of the reference
A_R	Optical density of the sample
A_S	Optical density of the reference
η_S	Refractive index of the sample
η_R	Refractive index of reference



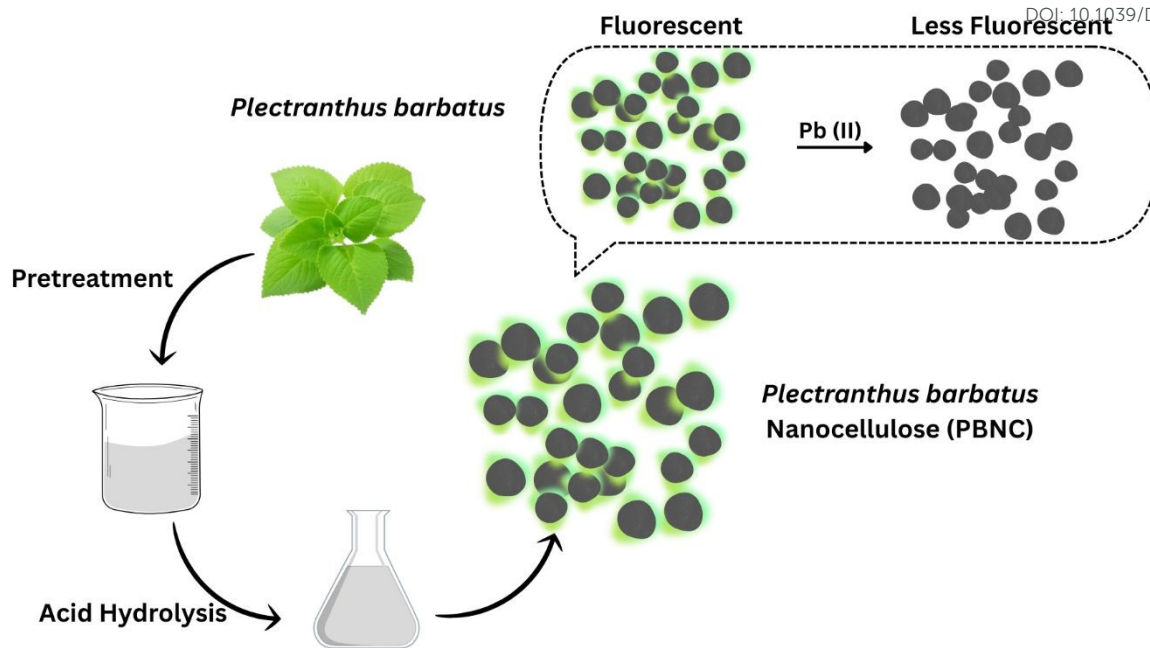


Fig.1 Schematic representation for the preparation of PBNC for the selective detection of Pb (II) ions.

2.5 Detection of Pb (II) ions

For the detection of Pb (II) ions, 20 μL of the aqueous dispersion of PBNC was added to the 3 ml of phosphate buffer solution of pH 7, followed by the serial addition (0-12 μL) of PbCl_2 of 10^{-5} M concentration. The PL spectra were recorded after incubating at room temperature for 5 minutes.

2.6 Evaluation of selectivity for Pb(II) in the presence interfering ions

The selectivity of PBNC toward Pb(II) ions was investigated in the presence of potentially interfering metal ions. Briefly, 3 mL of buffer solution was mixed with 20 μL of PBNC dispersion, followed by the simultaneous addition of 20 μL aqueous solutions of individual metal ion (Pb(II), Al(III), Ba(II), Fe(II), Hg(II), Mn(II), Na(I), and Ni(II)) solutions of 10^{-5} M concentration. A solution prepared without Pb(II) was used as the control. In a separate set of experiments, 3 mL of buffer solution containing 20 μL of PBNC and 20 μL of Pb(II) was prepared, after which 20 μL of each interfering metal ion solution (Al(III), Ba(II), Fe(II), Hg(II), Mn(II), Na(I), and Ni(II)) was added individually to evaluate possible interference effects. After incubation at room temperature for 5 min, the photoluminescence (PL) spectra were recorded.

2.7 Analysis of real samples

The practical applicability of the PBNC was tested through selective and sensitive detection of Pb(II) ions in lake water samples collected from Begur lake, Bangalore, India. The samples were pre-filtered using a 0.22 μm membrane to remove suspended particulates. Briefly, 3 mL aliquots of the filtered lake water were spiked with 20 μL of Pb(II) solutions at varying concentrations (10, 20, 30, 40, and 50 μM).

Subsequently, 20 μL of PBNC was added to each analyte solution, and the fluorescence response was recorded upon excitation at 220 nm.

3. Results and Discussion

We report the synthesis of fluorescent nanocellulose, PBNC, from the *Plectranthus barbatus* plant for the first time. Fluorescent PBNC was synthesised from *Plectranthus barbatus* via sequential mechanical processing, alkali delignification, bleaching, and H_2SO_4 hydrolysis, followed by dialysis and syringe filtration. PBNC was then used for the selective detection of Pb(II) ions in aqueous media. The resultant fluorescent PBNC was utilized for the selective detection of Pb (II) ions in aqueous solutions (Fig. 1).

3.1 Structural Characterisations at Different Stages of PBNC Synthesis

The XRD and FTIR analysis at the different stages of synthesis of *Plectranthus barbatus* nanocellulose were used to confirm the removal of lignin and hemicellulose and the enhancement in crystallinity.¹⁹ XRD analysis was carried out in order to analyse the increase in crystalline character during different synthesis stages of PBNC.²⁰ XRD of PBNC exhibited three distinct peaks near 2θ values of 16° , 22° , and 34° corresponding to the (110), (002), and (004) planes of cellulose (Fig. S1, Supplementary Information), which are characteristic crystalline peaks of cellulose.²¹ During the synthetic procedure, the raw *Plectranthus barbatus* plant underwent successive chemical treatments to transform into delignified and then to bleached forms. Each stage of treatment showed a significant increase in



the crystallinity, as evident from Fig. S1, Supplementary Information. This change in crystallinity is due to the chemical treatments that effectively removed amorphous components such as hemicellulose and lignin.²² The comparison of the XRD peaks at different synthesis steps of PBNC reveals that the delignification and bleaching reactions did not alter the structure of cellulose, but removed the amorphous content. The observed increase in crystallinity is a relative effect due to the removal of amorphous lignin and partial removal of hemicellulose.²³

The FTIR analysis was carried out to identify and characterize the functional groups in cellulose and nanocellulose.²⁴ Comparison of the FTIR spectra (Fig. S2, Supplementary Information) of raw *Plectranthus barbatus*, delignified fiber, and bleached fiber shows a clear increment in the cellulose content in bleached fiber in comparison with the other two stages. The spectra of the raw and delignified *Plectranthus barbatus* fiber were found to be almost similar. Similar peaks of raw and delignified stages suggest that the sodium hydroxide delignification process did not induce any significant chemical and structural changes.²⁵ A significant peak was found in the FTIR spectrum at 1490.27 cm^{-1} in both raw and delignified stages, which indicates the presence of the $-\text{CH}_2$ deformation vibration in side chains.²⁶ This peak is characteristic of lignin, and it is absent in the spectrum of the bleached state, suggesting the removal of lignin. The peaks at 1644.44 cm^{-1} and 1518.82 cm^{-1} correspond to the stretching vibrations of $\text{C}=\text{O}$ and the aromatic skeletal vibration of $\text{C}=\text{C}$ in lignin, respectively.²⁷ These peaks were also absent in the spectra of the bleached sample, indicating that the bleaching procedure using hydrogen peroxide and sodium hydroxide could successfully remove lignin.²⁸ However, a characteristic peak at 1587.34 cm^{-1} with notable intensity remained in the bleached samples, suggesting that the bleaching process did not fully eliminate the hemicellulose from the sample.²⁹ Additionally, peaks were observed in the spectra of the raw, delignified, and bleached samples at 3340.81 cm^{-1} for $-\text{OH}$ stretching vibration, 2894.91 cm^{-1} for $\text{C}-\text{H}$ stretching vibration, 1421.76 cm^{-1} for $-\text{CH}_2$, and $-\text{OCH}-$ plane bending vibrations, 1381.79 cm^{-1} for $\text{C}-\text{H}$ deformation vibration, and 907.87 cm^{-1} for anomeric carbon ($\text{C}1$) vibration.³⁰ These are all distinctive peaks of cellulose, demonstrating that highly pure cellulose was obtained. It is very much evident from the FTIR analysis that the characteristic peaks of bleached samples coincide with the reported FTIR peaks of cellulose, thus confirming the synthesis of pure cellulose from *Plectranthus barbatus*.

3.2 Structural Characterization of PBNC

HRTEM analysis was carried out to understand the structural and morphological characteristics of the nanocellulose.³¹ The TEM images (Fig. 2a) revealed the quasi-spherical morphology of the synthesised PBNC. The histogram (Fig. 2b) depicting the size distribution of PBNC shows that the average size is around 38 nm. The lattice fringe spacing of PBNC was found to be 0.58 nm, which corresponds to (002) plane of cellulose (Fig. 2c).³²

The Selected area electron diffraction (SAED) pattern of the PBNC clearly indicates that it is polycrystalline in nature, which is in accordance with XRD data (Fig. 2d).

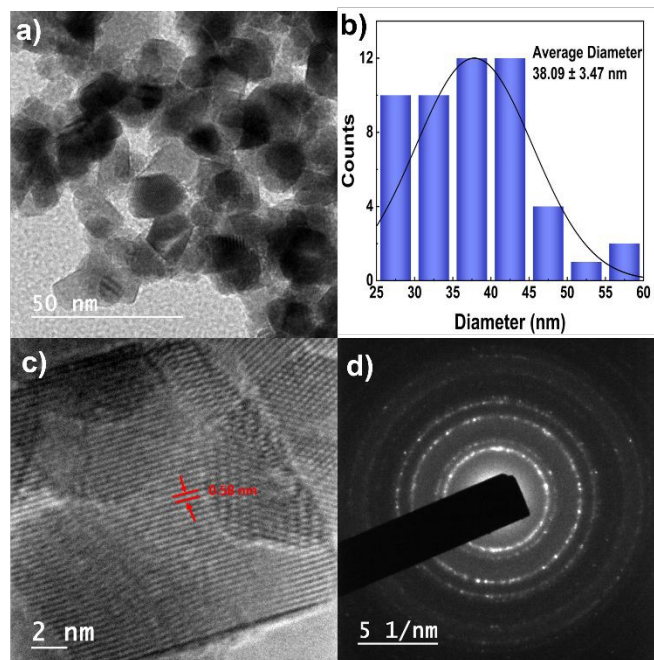


Fig. 2 a) TEM image of PBNC, b) size distribution histogram of PBNC, c) HRTEM image of PBNC, and d) SAED pattern obtained from PBNC.

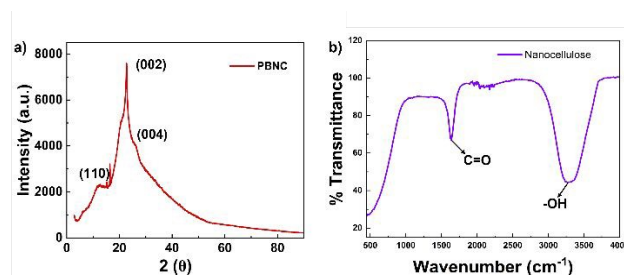


Fig. 3 a) XRD plot of PBNC with peaks corresponding to (002), (110) and (004) planes. b) FTIR spectra of PBNC, with peaks corresponding to carbonyl and hydroxyl groups.

The FTIR and XRD analysis of the PBNC were done to study the functional groups and crystallinity of synthesised PBNC nanocellulose.³³ Fig. 3a shows the XRD pattern of PBNC with a major peak at 22° and two minor peaks at 16° and 34° , corresponding to (002), (110) and (004) planes respectively.³⁴ The investigation of the FTIR spectrum of PBNC are in accordance with the data of previously reported nanocellulose.³⁵ The bands at or around 1520 cm^{-1} and 1230 cm^{-1} are often assigned to lignin and the peak at 1720 cm^{-1} to lignin and hemicellulose.³⁶ Upon the investigation of the FTIR spectra, we could find the absence of lignin and hemicellulose in PBNC. These findings confirm the synthesis of nanocellulose and also the absence of lignin and hemicellulose contents in the synthesised nanocellulose.³⁷ Zetapotential studies were carried out in nanocellulose in order to evaluate the surface charge characteristics and colloidal stability. The zetapotential of *Plectranthus barbatus* nanocellulose was found to be -26.7 mV ,



indicating moderate stability³⁸ (Fig. S3, Supplementary Information). The negative surface charge of the suspension minimizes the aggregation of the particles.³⁹

The characterisation techniques (FTIR, XRD and HRTEM) were selected to correlate the structural attributes of PBNC with its fluorescence behaviour and towards Pb(II) sensing performance. FTIR analysis confirms the presence of abundant oxygen-containing functional groups, which serve as active coordination sites for Pb(II) binding, thereby modulating fluorescence intensity.⁴⁰ XRD reveals the preservation of cellulose crystallinity following acid hydrolysis, indicating that the ordered crystalline regions contribute to structural stability which leads to enhanced surface accessibility for metal ion interaction.⁴¹ HRTEM demonstrates the formation of uniformly dispersed nanoparticles with large specific surface area, facilitating efficient Pb(II) adsorption and fluorescence response.⁴² Collectively, these results establish a structure–

property relationship, where surface chemistry of nanocellulose governs metal coordination, crystallinity supports optical stability, and nanoscale morphology promotes sensitivity, thereby justifying the relevance of FTIR, XRD, and TEM in elucidating the optical performance of PBNC as a fluoroprobe for Pb(II) ion sensing.

3.3 Optical Properties of PBNC and Sensing of Pb (II) Ions

Cellulose, the precursor of nanocellulose, is generally extracted from plant-based materials by removing lignin, hemicellulose and other organic matter. The luminescence in cellulose-containing materials was attributed to the presence of lignin (a small quantity of lignin residue was presumed to remain even after the synthesis of cellulose) or any other aromatic species generated during the synthesis process.⁴³ Casten and coworkers presented the theory that the phenylcoumarin and

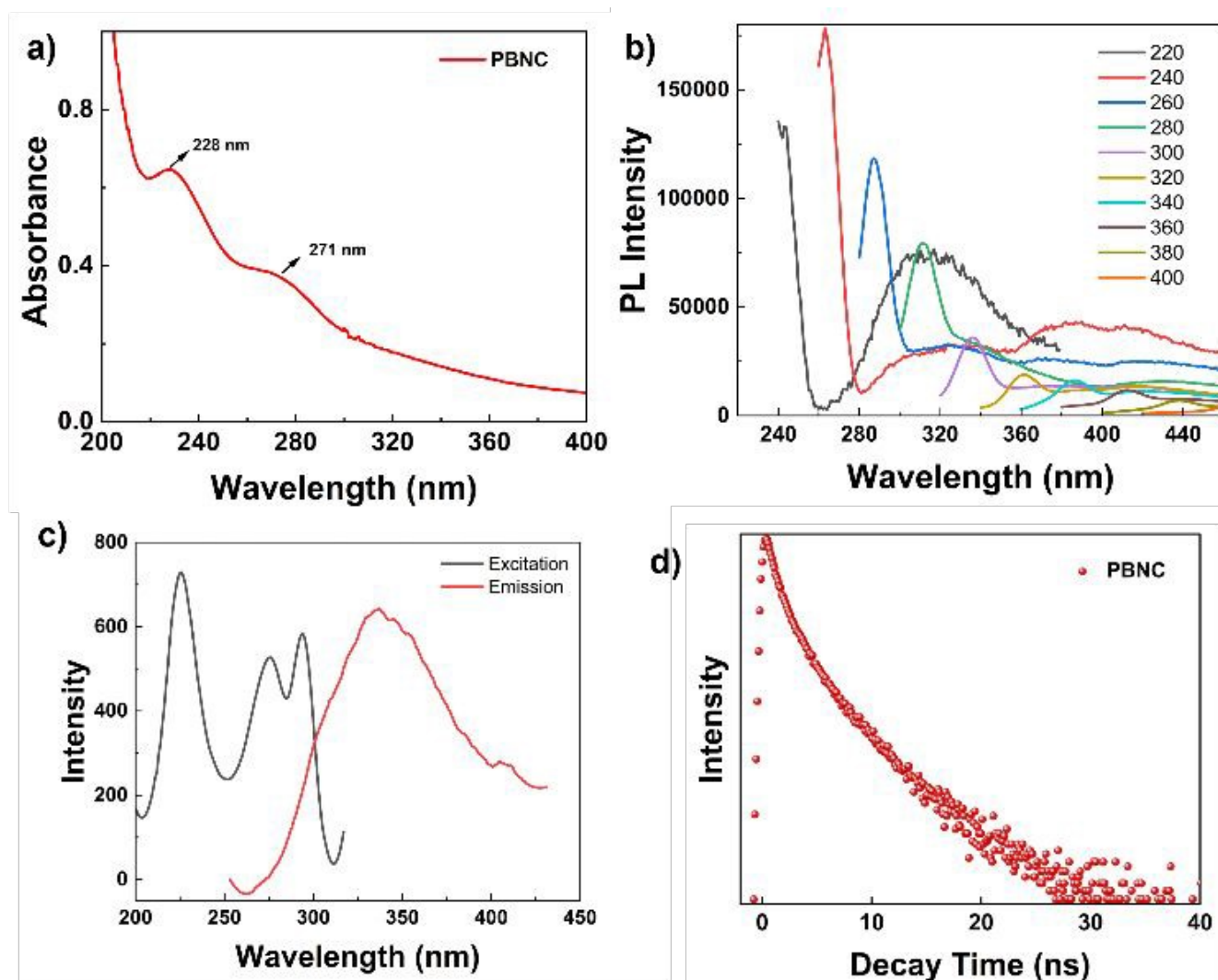


Fig. 4 a) UV-Visible absorption spectra of *Plectranthus barbatus* nanocellulose, b) The plot of excitation wavelength-dependent PL emissions of *Plectranthus barbatus* nanocellulose, and c) Excitation spectrum (emission at 315 nm) and emission spectrum ($\lambda_{ex} = 220$ nm), d) Plot of fluorescence life time of PBNC.



coniferyl structure of lignin is the reason for the fluorescence.⁴⁴ This understanding was questioned when Gray and Olmstead suggested, in 1993, that the luminescence in cellulose-based materials was due to the inherent property of cellulose.⁴⁵ The fluorescence of cellulose-based materials prepared from bacterial sources also negates the attribution of luminescence from lignin content, as bacterial sources are free from lignin.⁴⁶ Ding et. al came up with another explanation for the fluorescence of cellulose-based materials in early 2013.⁴⁷ They attributed the fluorescence to the glycosidic bond between glucose molecules present in the structure of cellulose.

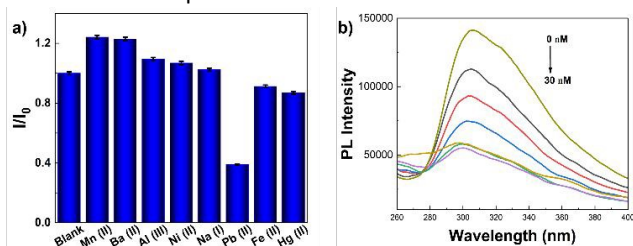


Fig.5 a) The PL response of PBNC to various metal ions, and b) The PL response of PBNC upon sequential addition of Pb (II) ions. I_0 and I are the PL intensities in the absence and presence of metal ions respectively at 315 nm ($\lambda_{ex} = 220$ nm). (Error amount, 3%; Y axis error bar of both \pm deviation).

The latest theory regarding the intrinsic fluorescence observed in cellulose-based materials is clustering-triggered emission (CTE).⁴⁸ The conjugate structures formed by the clustering of oxygen atoms are considered to be the reason for the intrinsic fluorescence of cellulose-based materials. This phenomenon is termed clustering-triggered emission (CTE), and it generally refers to the clustering of electron-rich heteroatoms and/or functional groups. These clusters are formed in a solid state or in an aggregated state, leading to effective overlap of electron clouds, thus lowering the energy gap and leading to efficient excitation. This clustering increases the conjugation length, leading to the formation of multiple cluster sizes with different energy gaps. The mechanism of clustered triggered emission is still contested. Main molecular interactions that are thought to facilitate the CTE mechanism are (a) overlap of lone pair (nonbonding) orbitals⁴⁹, (b) overlap of the lone pair and π orbitals⁵⁰, (c) dipole-dipole interactions⁵¹ and (d) simultaneous rigidification (via inter and intramolecular interactions)⁵², combined with clustering of delocalized electrons of various functional groups. The clustering of ether, hydroxyl and carbonyl units causes the delocalization of electron density in cellulose-based materials. These phenomena are believed to contribute to the fluorescence in cellulose materials.⁵³

The optical properties of PBNC were analysed using UV-Visible spectroscopy and PL spectroscopy. UV-Visible spectrum indicated two types of electronic transitions occurring in PBNC. The PBNC showed peaks at 228 nm (C=C) and 271 nm (C=O) in the UV-Visible absorption spectrum, corresponding to the transitions $\pi-\pi^*$ and $n-\pi^*$, respectively (Fig. 4a).⁵⁴ These transitions may arise due to the presence of π -conjugated domains or surface defects on PBNC. The absorption tail extending to the longer wavelength may arise from the low-

energy transitions of the functional groups present on the surface of the PBNC. The PBNC showed excitation wavelength dependent emissions when excited at different wavelengths ranging from 220 to 400 nm (Fig. 4b). The maximum emission (λ_{max}) is observed at 315 nm when the PBNC was excited at 220 nm (Fig. 4c). The quantum yield of PBNC was calculated to be 4.43%. The fluorescence lifetime of PBNC was found to be 0.6225 ns after fitting the decay curve with multi multi-exponential function (Fig. 4d). This indicates that PBNC has a short and multicomponent lifetime involving non non-radiative process⁵⁵.

3.4 Sensing of Pb (II) Ions using PBNC

The PL studies were performed on aqueous solutions of PBNC in the presence of Mn (II), Ba (II), Al (II), Ni (II), Na (I), Pb (II), Fe (II) and Hg (II) metal ions, under the same conditions. The fluorescence analysis revealed that the quenching response of PBNC is selective towards Pb (II) ions (38.9% of quenching upon addition of 20 μ l of 10^{-5} M Pb (II)) (Fig. 5a). There is no significant difference in the intensities with the other metal ions, which makes PBNC a potential sensor for the selective detection of Pb. versus the absorbance in y-axis. (II) ions.

The PL studies were conducted for the mixture of PBNC and selected set of metal ions (with and without Pb(II) ions) (Fig. 6a). The fluorescence studies were also conducted for (i) PBNC with various metal ions and Pb(II) ions, and (ii) PBNC with Pb(II) ions alone (Fig. 6b). From both the studies, it was confirmed that the quenching is selectively due to Pb(II) ions. This data further verifies specific interaction of the PBNC for Pb(II) ions, is primarily due to the specific binding interactions. From the above studies, PBNC were found to be capable of the selective detection of Pb(II), which makes it a potential candidate for a fluorescent probe.

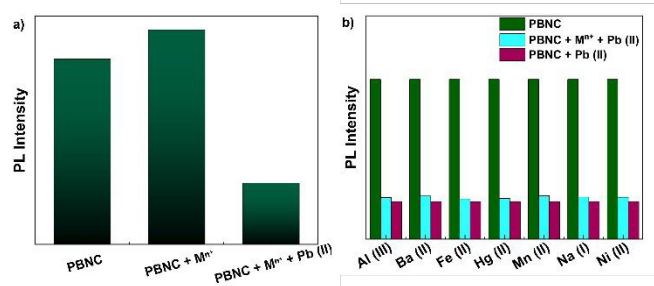


Fig. 6 a) The PL spectra of PBNC in response to the mixture of metal ions (Al(III), Ba(II), Fe(II), Hg(II), Mn(II), Na(I) and Ni(II)), both in the presence and absence of Pb (II) ions and b) the PL intensity at 315 nm of PBNC with other metal ions added with Pb(II) ions, and Pb (II) ions alone in PBNC respectively.

The PL intensity of PBNC quenched linearly with the increase in the concentration of Pb (II) ions within the range 0-30 nM. A linear distribution was observed between the concentration of Pb (II) ions and the fluorescence quenching of PBNC. With the increase in the concentration of Pb (II) ions, there occurred a substantial quenching response for PBNC. This linear quenching response of PBNC to Pb ions shows the sensitivity of PBNC towards Pb ions. (Fig. 5b)



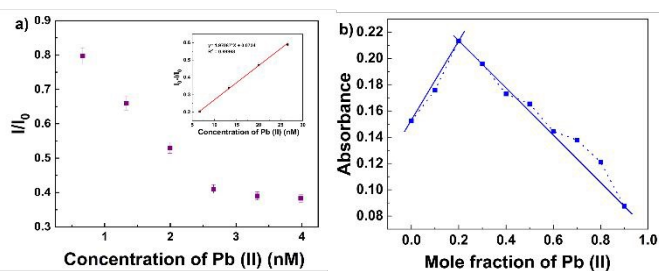


Fig. 7 a) The plot of I/I_0 against the concentration of Pb (II), inset shows the fitted plot in the lower concentrations. (Error amount, 3%; Y axis error bar of \pm deviation). b) Jobs plot was plotted using the mole fraction of Pb (II) ions in x-axis versus the absorbance in y-axis.

The fluorescence quenching followed the Stern-Volmer equation,⁵⁶ establishing a linear relationship between the relative intensity I/I_0 and concentration of Pb (II) with $R^2 = 0.99963$ (Fig. 7a). The detection limit of Pb (II) was calculated to be 2.7 nM. Job's plot analysis was used to study the binding of Pb (II) ions with the PBNC, by measuring the absorbance across different concentrations of of Pb (II) ions.⁵⁷

The stoichiometric ratio between Pb (II) ions and PBNC was determined using the Job's method of continuous variation, wherein a series of solutions were prepared by varying the mole fraction of Pb (II) (10^{-5} M) while maintaining a constant total molar concentration of the two components. The absorbance of each mixture was recorded after equilibrating it for 3 minutes, and the absorbance were plotted against the mole fraction of

Pb (II). Using the Jobs plot, the binding ratio of PBNC to Pb (II) ions was found to be 1: 0.2 (Fig. 7b).

The commonly proposed mechanisms to explain fluorescence quenching of the probe upon interaction with the analyte include static quenching, dynamic quenching, Förster resonance energy transfer (FRET), and the inner filter effect.⁵⁸ Static quenching arises from the formation of a non-fluorescent ground-state complex between the fluorophore and quencher; on the other hand, dynamic quenching results from collisional encounters between the excited fluorophore and quencher during its lifetime. Förster resonance energy transfer (FRET) involves a non-radiative energy transfer from the donor fluorophore to an acceptor when their spectral overlap and proximity are favorable. The inner filter effect, originates from the reabsorption or scattering of the excitation or emission light by the quencher.⁵⁹ These mechanisms may operate independently or simultaneously, and their contributions need to be assessed to rationalize the quenching behaviour of fluorescent systems. While a comprehensive mechanistic investigation into the fluorescence quenching of PBNCs by Pb (II) ions lies beyond the scope of this study, a scientifically grounded and plausible mechanism is nonetheless proposed to support the observed phenomena. In this study, the fluorescence quenching behavior of PBNCs in the presence of Pb (II) ions is predominantly ascribed to the inner filter effect, which is expected to play a central role in modulating the optical

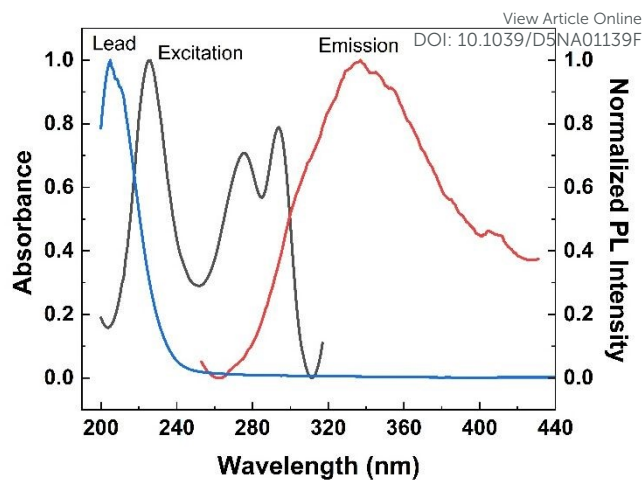


Fig. 8 The UV-Visible absorption spectrum of Pb (II) ions (blue), Excitation spectrum of PBNC (emission recorded at 315 nm) (black), Emission spectrum of PBNC ($\lambda_{ex} = 220$ nm) (red) respectively.

response of the system.^{60,61} This occurs due to the spectral overlap between the absorption band of Pb (II) ions and the excitation and/or emission bands of PBNC. As illustrated in Fig. 8, Pb (II) ions exhibit an absorption peak at 205 nm, while PBNC shows excitation and emission peaks at 220 nm and 315 nm, respectively. The pronounced spectral overlap between the absorption band of Pb (II) ions and the excitation band of PBNCs strongly substantiates the inner filter effect as a key mechanism responsible for the quenching of photoluminescence intensity upon interaction with Pb (II) ions.

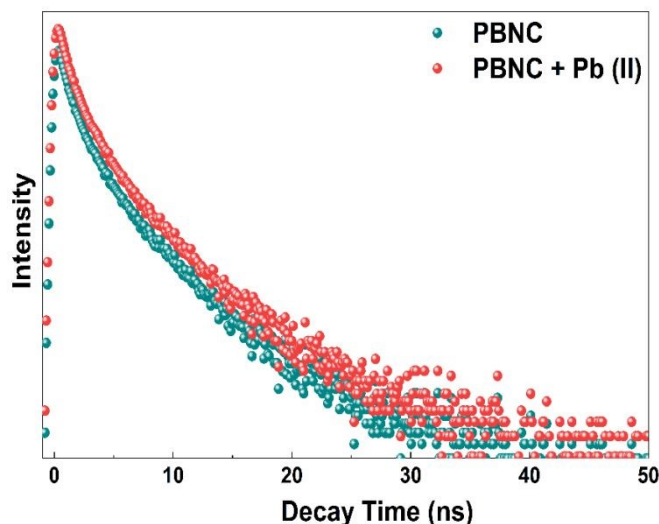


Fig. 9 Fluorescence lifetime of PBNC and PBNC in presence of Pb (II) ions

Also, the fluorescence lifetime of PBNC increased from 0.6225 ns to 1.240 ns upon addition of Pb (II) ions, while the PL intensity decreased significantly, as given in Fig 9. This behaviour rules out dynamic quenching, as dynamic processes reduce both PL intensity and lifetime simultaneously.⁶² The observed results indicate static quenching through ground-state complex formation between Pb (II) and oxygen-containing functional



ARTICLE

Journal Name

groups of PBNC. The formation of non-fluorescent PBNC–Pb (II) complexes reduces the number of emissive centers, leading to

View Article Online
DOI: 10.1039/D5NA01139F

Open Access Article. Published on 24 April 2026. Downloaded on 4/27/2026 5:17:09 PM.
This article is licensed under a Creative Commons Attribution–NonCommercial 3.0 Unported Licence.



Nanoscale Advances Accepted Manuscript

a decrease in PL intensity. Simultaneously, coordination of Pb (II) to PBNC modifies surface electronic states and suppresses fast non-radiative pathways, resulting in prolonged excited-state lifetime of the remaining emissive species.⁶³ Accordingly, the PL quenching of PBNC towards Pb (II) ions are attributed to a combination of static quenching and inner filter effect.

3.5 Real Water Sample Analysis

Sl. No.	Samples	Added (μM)	Found (μM)	Recovery (%)	RSD (% n=3)
1.	Lake water	10	10.16	101.60	4.33
		20	20.00	100.01	4.56
		30	29.86	99.56	5.27
		40	40.13	100.32	4.53
		50	49.91	99.83	5.23

The PBNC was used for the selective and sensitive detection of Pb ions in real water sample- lake water. The concentration of the Pb ions in the sample was below the detection limit of the proposed method, due to which different concentrations of Pb ions were spiked to the samples and used for fluorescent analysis. The spike recoveries for the quantitative determination of Pb ions in lake water were performed using PBNC by adding varying concentrations of Pb ions (10, 20, 30, 40, and 50 μM , respectively). The concentrations of Pb ions in the real samples were found (by linear fitting the plot of concentration of Pb ions versus the PL intensity (Fig. S4, Supplementary Information)), and the results are presented in Table 1. The Pb ion detection in real samples ranged from 99.83% to 101.60% at five spiked concentrations. The relative standard deviations (RSD) varied between 4.33 % and 5.27 %. This indicates the sensor has good accuracy and can be used for the detection of Pb(II) ions in the real samples.

4. Conclusions

In this work, a novel and efficient autofluorescent nanocellulose, PBNC, was synthesised from *Plectranthus barbatus* plant, a first of its kind, through optimized synthesis route. The inherent autofluorescent property of nanocellulose is used as an analytical signal to develop this optical sensor. PBNC was used to detect toxic Pb (II) ions in aqueous solutions based on fluorescence quenching mechanism. The quantum yield of PBNC was found to be 4.43%. The novelty of this study lies in utilizing the autofluorescence of PBNC, eliminating the need for incorporating additional sensing agents or fluorescent materials. Previous studies on fluorescence-based metal ion detection have primarily utilized nanocellulose as a supporting substrate rather than using it as an active sensing material.⁶⁴ PBNC as an autofluorescent nanocellulose was found to be simple, highly selective and sensitive, cost-effective, and free from the need for chemical modification. The fluorescence intensity of PBNC was quenched by Pb (II) ions, exhibiting a strong linear correlation between the fluorescence response and Pb (II) concentration, with a detection limit of 2.7 nM. These results implicate that PBNC can be employed to design and

develop effective fluoroprobe for metal ion detection without any further modifications. Such a sensor would be of low cost, sustainable, highly sensitive and selective and possess potential for many future innovations. The reported sensor can be upscaled for real-sample analysis and portable sensing formats, including paper-based devices and on-site detection kits for rapid Pb(II) sensing. Integration with smartphone-assisted fluorescence analysis could further enable point-of-care and field-deployable applications. In addition, systematic evaluation in complex environmental and biological matrices, alongside surface engineering for multi-ion recognition, may expand the scope of PBNC toward simultaneous detection of multiple heavy metals. Such developments are expected to advance plant-derived nanocellulose as a versatile, sustainable sensing material for next-generation environmental surveillance, water quality monitoring, and bioanalytical diagnostics.

Author contributions

Joshua Jose: Experimentation, Investigation, Data curation, Original draft, Writing, Review and Editing.

Aishwarya Joji Mathew: Experimentation, Investigation, Data curation, Original draft, Writing, Review and Editing.

Elizabeth Gabriel: Experimentation and Data curation.

Ancilin James: Experimentation and Data curation.

Vinod T. P.: Conceptualization, Validation, Resources, Visualization, Writing, Review and Editing, Funding acquisition, Project administration and Supervision.

Conflicts of interest

The authors declare that they have no known competing financial interests or personal relationships that could have appeared to influence the work reported in this paper.

Data availability

Data will be made available on request.

Acknowledgements

Joshua Jose and Aishwarya Joji Mathew are grateful to Christ University for the research fellowship. Vinod T. P. is thankful to Centre for Research Projects (CRP), Christ University, for the Seed Money Grant SMSS-2334. The authors are thankful to Vision Group on Science and Technology (VGST), Govt. of Karnataka for K-FIST-L1 grant (GRD No. 1143).

References

- 1 P. Kumar Gupta, S. Sai Raghunath, D. Venkatesh Prasanna, P. Venkat, V. Shree, C. Chithanathan, S. Choudhary, K. Surender and K. Geetha, in *Cellulose*, IntechOpen, 2019.
- 2 R. Kamel, N. A. El-Wakil, A. Dufresne and N. A. Elkasabgy, *International Journal of Biological Macromolecules*, 2020, **163**, 1579–1590.



- 3 H. Sharifi, J. Tashkhourian and B. Hemmateenejad, *Analytica Chimica Acta*, 2020, **1126**, 114–123.
- 4 F. L. MIGLIORINI, K. B. R. TEODORO and D. S. CORREA, *Cellulose Chemistry and Technology*, 2020, **54**, 407–413.
- 5 M. V. Santos, F. E. Maturi, É. Pecoraro, H. S. Barud, L. R. Lima, R. A. S. Ferreira, L. D. Carlos and S. J. L. Ribeiro, *Frontiers in Bioengineering and Biotechnology*, DOI:10.3389/fbioe.2021.617328.
- 6 L. Donaldson, *Molecules*, 2020, **25**, 2393.
- 7 H. Zhang and B. Z. Tang, *JACS Au*, 2021, **1**, 1805–1814.
- 8 Z. Wang, H. Zhang, S. Li, D. Lei, B. Z. Tang and R. Ye, *Topics in Current Chemistry*, 2021, **379**, 14.
- 9 Y. Wang, Z. Zhao and W. Z. Yuan, *ChemPlusChem*, 2020, **85**, 1065–1080.
- 10 L. Gan, N. Feng, S. Liu, S. Zheng, Z. Li and J. Huang, *Particle & Particle Systems Characterization*, DOI:10.1002/ppsc.201800412.
- 11 K. B. R. Teodoro, M. J. Silva, R. S. Andre, R. Schneider, M. A. Martins, L. H. C. Mattoso and D. S. Correa, *Carbohydrate Polymers*, 2024, **324**, 121494.
- 12 K. Kulbat-Warycha, J. Oracz and D. Żyzelewicz, *Molecules*, DOI:10.3390/molecules27248986.
- 13 J. Wu, T. Wang, Y. Zhang and W.-P. Pan, *Bioresource Technology*, 2019, **291**, 121859.
- 14 M. F. Cordeiro, T. R. S. Nunes, F. G. Bezerra, P. K. M. Damasco, W. A. V. Silva, M. R. A. Ferreira, O. M. C. Magalhães, L. A. L. Soares, I. M. F. Cavalcanti, M. G. R. Pitta and M. J. B. M. Rêgo, *Brazilian Journal of Biology*, DOI:10.1590/1519-6984.236297.
- 15 J. Jose and T. P. Vinod, *New Journal of Chemistry*, DOI:10.1039/D5NJ01022E.
- 16 L. U. S. Faria, B. J. S. Pacheco, G. C. Oliveira and J. L. Silva, *Journal of Materials Research and Technology*, 2020, **9**, 12346–12353.
- 17 W. J. Orts, J. Shey, S. H. Imam, G. M. Glenn, M. E. Guttman and J.-F. Revol, *Journal of Polymers and the Environment*, 2005, **13**, 301–306.
- 18 B. Zhu, S. Sun, Y. Wang, S. Deng, G. Qian, M. Wang and A. Hu, *J. Mater. Chem. C*, 2013, **1**, 580–586.
- 19 M. N. Khan, N. Rehman, A. Sharif, E. Ahmed, Z. H. Farooqi and M. I. Din, *International Journal of Biological Macromolecules*, 2020, **153**, 72–78.
- 20 K. S. Prado and M. A. S. Spinacé, *International Journal of Biological Macromolecules*, 2019, **122**, 410–416.
- 21 R. Chen, Q. Zhang, Y. Gu, L. Tang, C. Li and Z. Zhang, *Analytica Chimica Acta*, 2015, **853**, 579–587.
- 22 J. Liang, B. Liu, X. Li, X. Mo, C. Qin, C. Liang, C. Huang and S. Yao, *Bioresource Technology*, 2023, **384**, 129328.
- 23 S. Si, Y. Chen, C. Fan, H. Hu, Y. Li, J. Huang, H. Liao, B. Hao, Q. Li, L. Peng and Y. Tu, *Bioresource Technology*, 2015, **183**, 248–254.
- 24 R. Koshani, J. E. Eiyegbenin, Y. Wang and T. G. M. van de Ven, *Journal of Colloid and Interface Science*, 2022, **607**, 134–144.
- 25 W. Jung, D. Savithri, R. Sharma-Shivappa and P. Kolar, *Energies*, 2018, **11**, 376.
- 26 Y. Song, J. Zhang, X. Zhang and T. Tan, *Bioresource Technology*, 2015, **193**, 164–170.
- 27 X. Li, Y. Ding, X. Pan, Y. Xing, B. Zhang, X. Liu, Y. Tan, H. Wang and C. Li, *Journal of Energy Chemistry*, 2022, **67**, 492–499.
- 28 H. Du, M. Parit, K. Liu, M. Zhang, Z. Jiang, T.-S. Huang, X. Zhang and C. Si, *ACS Applied Materials & Interfaces*, 2021, **13**, 32115–32125.
- 29 Y. C. Ching and T. S. Ng, *BioResources*, 2014, **9**, 6373–6385.
- 30 K. Liu, H. Du, T. Zheng, H. Liu, M. Zhang, R. Zhang, H. Li, H. Xie, X. Zhang, M. Ma and C. Si, *Carbohydrate Polymers*, DOI:10.1016/j.carbpol.2021.117740.
- 31 Y. Zhu, Z. Wei, F. Jiang, W. Hu, X. Yu and S. Du, *Carbohydrate Polymers*, 2024, **342**, 122419.
- 32 A. Kumar, S. Asu, P. Mukherjee, P. Singh, A. Kumari and S. K. Sahu, *Journal of Photochemistry and Photobiology A: Chemistry*, 2021, **406**, 113019.
- 33 Q. Qin, X. Zhang, B. Gao, W. Liu, L. Han, S. L. Sing and X. Liu, *International Journal of Biological Macromolecules*, 2024, **257**, 127944.
- 34 K. J. Mintz, M. Bartoli, M. Rovere, Y. Zhou, S. D. Hettiarachchi, S. Paudyal, J. Chen, J. B. Domena, P. Y. Liyanage, R. Sampson, D. Khadka, R. R. Pandey, S. Huang, C. C. Chusuei, A. Tagliaferro and R. M. Leblanc, *Carbon*, 2021, **173**, 433–447.
- 35 H. Du, C. Liu, Y. Zhang, G. Yu, C. Si and B. Li, *Industrial Crops and Products*, 2016, **94**, 736–745.
- 36 V. S. Borovkova, Y. N. Malyar, I. G. Sudakova, A. I. Chudina, D. V. Zimonin, A. M. Skripnikov, A. V. Miroshnikova, V. A. Ionin, A. S. Kazachenko, V. V. Sychev, I. S. Ponomarev and N. Issaoui, *Polymers*, 2022, **14**, 4521.
- 37 A. Barhoum, J. Jeevanandam, A. Rastogi, P. Samyn, Y. Boluk, A. Dufresne, M. K. Danquah and M. Bechelany, *Nanoscale*, 2020, **12**, 22845–22890.
- 38 W. Huo, X. Zhang, K. Gan, Y. Chen, J. Xu and J. Yang, *Journal of the European Ceramic Society*, 2019, **39**, 574–583.
- 39 R. R. Retamal Marín, F. Babick and L. Hillemann, *Colloids and Surfaces A: Physicochemical and Engineering Aspects*, 2017, **532**, 516–521.
- 40 H. Xu, M. Yan, W. Li, H. Jiang and L. Guo, *Water Research*, 2018, **144**, 435–443.
- 41 A. Grząbka-Zasadzińska, I. Ratajczak, K. Król, M. Woźniak and S. Borysiak, *Cellulose*, 2021, **28**, 5745–5759.
- 42 A. Abdullah, A. N. Kursunlu and E. Guler, *RSC Advances*, 2023, **13**, 2683–2691.
- 43 J. Poisson and K. Zhang, *Accounts of Materials Research*, 2024, **5**, 920–932.
- 44 B. Albinsson, S. Li, K. Lundquist and R. Stomberg, *Journal of Molecular Structure*, 1999, **508**, 19–27.
- 45 J. A. Olmstead and D. G. Gray, *Journal of Photochemistry and Photobiology A: Chemistry*, 1993, **73**, 59–65.
- 46 R. Stephen Davidson, L. A. Dunn, A. Castellan and A. Nourmamode, *Journal of Photochemistry and Photobiology, A: Chemistry*, 1991, **58**, 349–359.
- 47 Q. Ding, W. Han, X. Li, Y. Jiang and C. Zhao, *Scientific Reports*, 2020, **10**, 21387.
- 48 Y. Gong, Y. Tan, J. Mei, Y. Zhang, W. Yuan, Y. Zhang, J. Sun and B. Z. Tang, *Science China Chemistry*, 2013, **56**, 1178–



- 1182.
- 49 J. Wang, L. Xu, S. Zhong, Y. Yang, G. Feng, Q. Meng, Y. Gao and X. Cui, *Polymer Chemistry*, 2021, **12**, 7048–7055.
- 50 P. Liao, J. Huang, Y. Yan and B. Z. Tang, *Materials Chemistry Frontiers*, 2021, **5**, 6693–6717.
- 51 W. Xu, D. Hu, Z. Wang, G. Wang, K. Liu, J. Liang, R. Miao and Y. Fang, *The Journal of Physical Chemistry Letters*, 2022, **13**, 5358–5364.
- 52 Q. Zhou, B. Cao, C. Zhu, S. Xu, Y. Gong, W. Z. Yuan and Y. Zhang, *Small*, 2016, **12**, 6586–6592.
- 53 S. Tang, T. Yang, Z. Zhao, T. Zhu, Q. Zhang, W. Hou and W. Z. Yuan, *Chemical Society Reviews*, 2021, **50**, 12616–12655.
- 54 J. Kim, H. J. Shim, J. Yang, M. K. Choi, D. C. Kim, J. Kim, T. Hyeon and D. Kim, *Advanced Materials*, DOI:10.1002/adma.201700217.
- 55 Z. Zhang, G. Liu, X. Li, S. Zhang, X. Lü and Y. Wang, *ChemPlusChem*, 2020, **85**, 487–502.
- 56 X. Zhou, X. Gao, M. Liu, C. Wang and F. Chu, *Microchimica Acta*, 2017, **184**, 4175–4181.
- 57 S. Shanmuga Priya and S. Suseem, *RSC Advances*, 2024, **14**, 17471–17479.
- 58 F. Zu, F. Yan, Z. Bai, J. Xu, Y. Wang, Y. Huang and X. Zhou, *Microchimica Acta*, 2017, **184**, 1899–1914.
- 59 L. Pei, W. Zhang, S. Yang, K. Chen, X. Zhu, Y. Zhao and S. Han, *Journal of Fluorescence*, 2023, **33**, 1147–1156.
- 60 M. Zheng, Z. Xie, D. Qu, D. Li, P. Du, X. Jing and Z. Sun, *ACS Applied Materials & Interfaces*, 2013, **5**, 13242–13247.
- 61 A. J. Mathew, T. P. Vinod and Y. Nair, *Nanoscale Advances*, DOI:10.1039/D5NA00892A.
- 62 G. Hollett, D. S. Roberts, M. Sewell, E. Wensley, J. Wagner, W. Murray, A. Krotz, B. Toth, V. Vijayakumar and M. J. Sailor, *The Journal of Physical Chemistry C*, 2019, **123**, 17976–17986.
- 63 D. Genovese, M. Cingolani, E. Rampazzo, L. Prodi and N. Zaccheroni, *Chemical Society Reviews*, 2021, **50**, 8414–8427.
- 64 T. Park, N. Kim, D. Kim, S.-W. Kim, Y. Oh, J.-K. Yoo, J. You and M.-K. Um, *ACS Applied Materials & Interfaces*, 2019, **11**, 48239–48248.

View Article Online
DOI: 10.1039/D5NA01139F



Fluorescent Nanocellulose Derived from *Plectranthus barbatus* for the Selective Detection of Pb (II) Ions in Aqueous Solutions

*Joshua Jose, Aishwarya Joji Mathew, Elizabeth Gabriel, Ancilin James and Vinod T. P.**

The data supporting this article have been included as part of the Supplementary Information. (Fig. S1. XRD plot of the different synthesis stages of PBNC, Fig. S2. FTIR plot of different synthesis stages of PBNC, and Fig. S3. Zeta potential graph of PBNC.)

